Temperature-dependent Phase Behavior of the Thermoresponsive Polymer Poly(*N*-isopropylmethacrylamide) in Aqueous Solution

Chia-Hsin Ko[1], *Kora-Lee Claude*[1], *Bart-Jan Niebuur*[1], *Florian A. Jung*[1], *Jia-Jhen Kang*[1], *Dirk Schanzenbach*[2], *Henrich Frielinghaus*[3], *Lester C. Barnsley*[3,8], *Baohu Wu*[3], *Vitaliy Pipich*[3], *Alfons Schulte*[4], *Peter Müller-Buschbaum*[5,6], *André Laschewsky*[2,7], *Christine M. Papadakis*[1,*]

[1]Technische Universität München, Physik-Department, Fachgebiet Physik weicher Materie, James-Franck-Straße 1, 85748 Garching, Germany

[2]Institut für Chemie, Universität Potsdam, Karl-Liebknecht-Straße 24-25, 14476 Potsdam-Golm, Germany

[3]Jülich Centre for Neutron Science (JCNS) at Heinz Maier-Leibnitz Zentrum (MLZ), Forschungszentrum Jülich GmbH, Lichtenbergstraße 1, 85748 Garching, Germany

[4]University of Central Florida, Department of Physics and College of Optics and Photonics, 4111 Libra Drive, Orlando, FL 32816-2385, U.S.A.

[5]Technische Universität München, Physik-Department, Lehrstuhl für Funktionelle Materialien, James-Franck-Straße 1, 85748 Garching, Germany

[6]Heinz Maier-Leibnitz Zentrum (MLZ), Technische Universität München, Lichtenbergstr. 1, 85748 Garching, Germany

[7]Fraunhofer-Institut für Angewandte Polymerforschung, Geiselbergstraße 69, 14476 Potsdam-Golm, Germany

[8]Australian Synchrotron, ANSTO, 800 Blackburn Road, Clayton 3168, Australia

KEYWORDS. Phase transition, thermoresponsive polymers, poly(*N*-isopropylmethacrylamide), differential scanning calorimetry, Raman spectroscopy, small-angle neutron scattering, very small-angle neutron scattering

ToC Graphics.

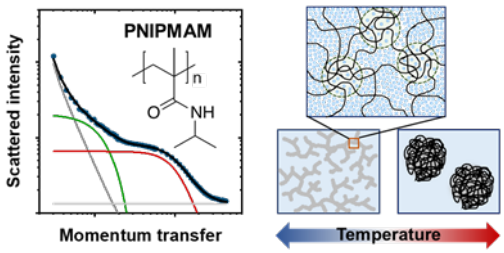

ABSTRACT. Poly(*N*-isopropylmethacrylamide) (PNIPMAM) is a thermoresponsive polymer, exhibiting lower critical solution temperature (LCST) behavior in aqueous solution. We investigate the temperature-dependent phase behavior of PNIPMAM solutions in D_2O using turbidimetry, differential scanning calorimetry (DSC), small-angle and very small-angle neutron scattering (SANS and VSANS), and Raman spectroscopy, covering a large concentration range

and compare the results from PNIPMAM with the findings from its analogue poly(*N*-isopropylacrylamide) (PNIPAM). We find that the PNIPMAM chains only dehydrate 2-3 °C above the macroscopic cloud point temperature, T_{CP}. Even in the one-phase state, loosely packed, large-scale inhomogeneities and physical crosslinks are observed, and the chain conformation of PNIPMAM is more compact than the one of PNIPAM. This is attributed to the attractive intermolecular interactions between the hydrophobic moieties. The phase transition of PNIPMAM is broader than the one of PNIPAM. Upon heating to the two-phase state, the PNIPMAM chains collapse and form mesoglobules. These are larger and more hydrated than for PNIPAM. This is attributed to the steric hindrance caused by the additional methyl groups, which weaken the intrapolymer interactions in the two-phase state. Thus, the methyl groups in the backbone of the PNIPMAM chains have a significant impact on the hydration and the structural behavior around the phase transition.

1. Introduction

Thermoresponsive polymers in aqueous solution have been amply studied because they are of interest for applications requiring a temperature induced switchable behavior.[1-3] The widely inverstigated thermoresponsive polymer poly(*N*-isopropylacrylamide) (PNIPAM), for instance, has a sharp collapse transition at ~32 °C in a wide range of molar masses and concentrations, i.e. it shows lower critical solution temperature (LCST) behavior of the so-called type II behavior.[4, 5] Upon heating through the cloud point (T_{CP}), the chains dehydrate strongly and form mesoglobules.[5-9] These contain only little water and are long-lived, which was attributed to the viscoelastic effect among others.[10-12] PNIPAM has the ability to form hydrogen bonds, both with water and with other PNIPAM repeat units.[13-16] The LCST behavior of PNIPAM has been

attributed to the delicate balance between hydrogen bonding with water and hydrophobic hydration.[17, 18]

Poly(*N*-isopropylmethacrylamide) (PNIPMAM) is very similar to PNIPAM, despite an additional methyl group on the backbone. As PNIPAM, it shows LCST-behavior of type II in aqueous solution, but with a higher coil-to-globule collapse transition at ~44 °C, which depends only weakly on molar mass, concentration, and added electrolytes.[5, 19]

The molecular origin of the counter-intuitive increase of the T_{CP} of PNIPMAM is still under discussion. It seems to be related to the steric demand of the methyl group altering the chain conformation and the hydration behavior. PNIPMAM solutions were investigated intensively by turbidimetry,[20-24] differential scanning calorimetry (DSC),[24-26] Fourier transform infrared spectroscopy (FTIR),[27-29] nuclear magnetic resonance (NMR),[29] Raman spectroscopy,[28] and light scattering. It was found that, below T_{CP}, the PNIPMAM chains are more hydrated and expanded than PNIPAM chains,[30] and that, above T_{CP}, the aggregates are more loosely packed than the ones formed by PNIPAM.[26] Molecular dynamics simulations and quantum mechanical calculations revealed that both the intermolecular interactions and the intramolecular interactions among the amide groups from PNIPMAM are weaker than the ones from PNIPAM, which is attributed to the steric hindrance caused by the additional methyl groups.[28, 31] Thus, small changes in the molecular structure can strongly alter the behavior around the coexistence line.

We previously investigated a $PNIPMAM_{195}$ sample in a 50 g L^{-1} solution in D_2O.[32] A low value of T_{CP} was found, namely 38.0 °C, which we attributed to the rather hydrophobic fluorescence tag used for molar mass characterization. Below T_{CP}, the small-angle neutron scattering (SANS) data were significantly more complex than the ones of PNIPAM. In addition to the usually observed chain scattering, inhomogeneities at intermediate length scales and large aggregates were

observed. Just above T_{CP}, scattering from single chains and from large, compact aggregates was found. Only far above T_{CP}, single chain scattering was strongly reduced, and very large, compact aggregates prevailed. These phenomena had not been observed in PNIPAM solutions and were attributed to an enhanced hydrophobic effect due to the additional methyl groups.

Even though a number of studies have addressed the behavior of PNIPMAM in aqueous solution, in most cases, only single samples were studied with only few characterization methods. In this work, we present a systematic study of the phase behavior of PNIPMAM in aqueous solution in a wide concentration range (2-150 g L^{-1}). A number of techniques address different aspects of the phase transition: The T_{CP} values are determined using turbidimetry and optical microscopy. The thermal signature of the transition is characterized by differential scanning calorimetry (DSC). SANS and very small-angle neutron scattering (VSANS) give structural information on a wide range of length scales. Raman spectroscopy gives insight into the hydrophobic hydration behavior around the T_{CP}. Finally, all observations are combined to give a comprehensive picture of the structural changes around the phase transition.

2. Experimental Section

Materials. A poly(*N*-isopropylmethacrylamide) (PNIPMAM) homopolymer with the apparent number average molar mass M_n^{app} = 17,000 g mol^{-1} (equivalent to the apparent number average degree of polymerization of 133) and a dispersity index $Đ$ = 1.74 was synthesized by free radical polymerization (FRP). A 15 % (w/w) monomer solution in THF was thoroughly deoxygenated by bubbling with argon for 30 min and then polymerized with 0.5 mol-% of 2,2′-azobis(2-methylpropionitrile) (AIBN) based on the monomer for 18 h at 60 °C. The resulting polymer was precipitated three times into a diethyl ether-hexane mixture, filtered, dissolved in water and

lyophilized (yield 59 %). ^{1}H NMR analysis showed no remaining monomer in the product. Values of M_n^{app} and $Đ$ were determined by size exclusion chromatography (SEC) using *N*-methyl-2-pyrrolidone (NMP) with 0.5 % LiBr as eluent (TSP P1000 pump, Shimadzu RID-6A detector, columns PSS GRAL precolumn 10 µm 8x50 mm, PSS GRAM linear column 7 µm 8x300 mm). Calibration was done using narrowly dispersed polystyrene standards. For all measurements, $PNIPMAM_{133}$ was dissolved in D_2O (Deutero GmbH, purity 99.95%, Kastellaun, Germany) at concentrations between 2 and 150 g L^{-1}. All solutions were left to equilibrate at room temperature for at least 48 h.

Cloud Point Determination. To identify the cloud points, turbidimetry was performed using a 10 mW HeNe laser with a wavelength of 632.8 nm and a Si photodiode (Thorlabs, CITY). The samples were loaded in quartz glass cells (Hellma Analytics) with a light path of 1 mm. The cells were inserted into an aluminum sample stage connected to a Julabo F12 thermostat (Julabo GmbH, Seelbach, Germany). Temperature scans were carried out at a heating rate of 0.2 K min^{-1}. A Pt100 resistance thermosensor was directly attached to the sample stage. The transmitted light intensity was normalized to the maximum measured intensity to give the transmission. The transmission decreases abruptly at the cloud point temperature T_{CP}, which was taken as the onset temperature of the decaying transmission.

Differential Scanning Calorimetry (DSC). DSC measurements were conducted using a DSC 3 STAR^{e} system from Mettler Toledo. The system was calibrated using indium and zinc. Nitrogen gas with a flow rate of 50 ml min^{-1} was employed as a standard atmosphere. Aqueous solutions of PNIPMAM were filled in a 40 µL aluminum pan. The reference sample was an empty aluminum pan of identical size. The measurements were carried out in a temperature range of 10-80 °C. Each sample firstly underwent a heating and cooling cycle with a rate of 10 K min^{-1} to erase the thermal

history. The characteristic temperatures were determined from the second heating scan, carried out at a rate of 1 K min^{-1}. The onset temperature of the phase transition was defined by the intersection of the extrapolated baseline with the tangent of the peak. The peak temperature was taken at the maximum of the endothermic peak. The enthalpy of the phase transition was obtained from the area under the endothermic or exothermic peak and was normalized to the mass of the polymer solution in the unit of J g_s^{-1}.

Optical Microscopy (OM) and Raman Spectroscopy. Optical microscopy and Raman spectroscopy were carried out using the setup described in ref. 9. The Raman spectra were acquired using a LabRam HR 800 system (JY Horiba). A HeNe laser with a wavelength of 632.8 nm was used as the excitation source. The spectra were recorded at a resolution of 2 cm^{-1}. The laser power at the sample position was less than 3 mW at a spot size of 1.5 μm. The polymer solution was loaded in a fused silica micro capillary with square cross-section (edge length 100 μm). The capillary was embedded in a copper stage connected to a circulating water bath thermostat. The sample temperature was measured by a Pt100 resistance thermosensor attached to the copper stage. Each spectrum was obtained with an integration time of 120 s. The dark current was subtracted before the deconvolution of the spectra. The resulting Raman spectra in the frequency region of 2200 to 3100 cm^{-1} were fitted by a superposition of three Gaussian functions assigned to several OD-vibration modes and four Lorentzian functions attributed to various CH-stretching modes. An example of deconvolution of frequency range from 2200 to 3100 cm^{-1} is shown in Figure S7 in the Supporting Information (SI). We aim to focus on the hydrophobic interactions in the CH-stretching region with frequency range from 2850 to 3100 cm^{-1} (Figure S8 in the SI). The Gaussian functions were only used to account for the possible overlap of the OD-vibration modes with the CH-stretching region, and are not supposed to give a precise description of the vibration modes in

water in the OD-vibration region. Therefore, only the spectral bands in the CH-stretching region with frequency range from 2850 to 3100 cm^{-1} are further discussed.

Before each measurement of a Raman spectrum, an OM image was taken in the same setup using an Olympus X41 microscope equipped with a CCD camera. Heating scans were conducted from 24 to 50 °C in steps of 1-2 °C with a thermal equilibration time of 5 min before each measurement. T_{CP} was determined as the average temperature between the temperature just before mesoglobules appeared and the temperature at which mesoglobules were present as observed by OM. We note that there is a small offset in the temperature measured by the Pt100 resistance thermosensor and the sample temperature with the latter being a few °C lower, which is possibly due to heat losses of the microscope objective.

Small-Angle Neutron Scattering (SANS). SANS measurements of PNIPMAM solutions in D_2O having concentrations of 30, 100 and 150 g L^{-1} were performed at the instrument KWS-1 operated by the Jülich Centre for Neutron Science (JCNS) at Heinz-Meier-Leibnitz Zentrum (MLZ), Garching, Germany.[33, 34] The neutron wavelength was λ = 0.50 nm with a spread $\Delta\lambda/\lambda$ = 0.1. The sample-detector distances were 1.5, 8.0 and 20 m, resulting in a q range of 0.03 – 4.4 nm^{-1}. $q = 4\pi \sin(\theta/2)/\lambda$ is the momentum transfer with θ being the scattering angle. Samples were mounted in quartz glass cells (Hellma Analytics) with a light path of 1 mm. A Peltier thermostated sample stage was used. The measurement times were 5 min at 1.5 m, 20 min at 8 m, and 30 min at 20 m. The sample transmission was measured and taken into account. Plexiglass was measured to determine the detector sensitivity and bring the data to the absolute intensity. The background scattering from the empty cell and the dark current measured using boron carbide were subtracted and calibrated. All data operations including azimuthal averaging were carried out using standard procedures in the software QtiKWS provided by JCNS.

Very Small-Angle Neutron Scattering (VSANS). VSANS measurements were carried out at the instrument KWS-3 operated by the Jülich Centre for Neutron Science (JCNS) at Heinz-Meier-Leibnitz Zentrum (MLZ), Garching, Germany.[35] The incident neutrons had a wavelength of 1.28 nm with a spread $\Delta\lambda/\lambda$ of 0.18. Using a sample-detector distance of 9.4 m, a q range of 0.002 – 0.02 nm^{-1} was covered. The neutron path of the quartz glass cells (Hellma Analytics) was 2 mm for 100 and 150 g L^{-1}, and 1 mm for 30 g L^{-1}. An aluminum sample stage with water bath circulation was used to control the temperature. The measurement time was 20 min, except for 30 g L^{-1}, where it was 25 min. Plexiglass was used as a standard for the absolute intensity calibration and the detector sensitivity. The dark current, measured using boron carbide as well as the background scattering from the empty cell were subtracted. All the data processing was carried out using standard procedures in the software QtiKWS. The neutron transmission was measured during the VSANS measurements using the direct beam on the detector. T_{CP}^{VSANS} was defined as the temperature at which the transmission starts to decay.

In SANS and VSANS measurements, the PNIPMAM solutions were measured while heating from 30 to 53 °C in steps of 1-3 °C. After each temperature change, the sample was equilibrated for 20 min.

Analysis of SANS Curves. In the one-phase state, the SANS curves of PNIPMAM solutions were fitted by the following model function:

$$\boldsymbol{I(q) = I_{agg}(q) + I_{gel}(q) + I_{fluct}(q) + I_{bkg}} \quad (1)$$

$I_{agg}(q)$ denotes the forward scattering caused by the large-scale inhomogeneities. $I_{gel}(q)$ characterizes the physical crosslinks in PNIPMAM solutions. $I_{fluct}(q)$ is a modified Ornstein-Zernike term, describing the concentration fluctuations in semidilute polymer solutions, and I_{bkg} is a constant incoherent background.

In most cases, $I_{agg}(q)$ was approximated by a modified Porod term,[36]

$$I_{agg}(q) = \frac{K_P}{q^{\alpha}} \quad (2)$$

which gives a scaling factor, K_P and the Porod exponent, α. In the one-phase state, the Porod term describes large-scale inhomogeneities, which were described as large mass fractals. The Porod exponent α indicates the fractal dimension of large-scale inhomogeneities.[37]

The gel term $I_{gel}(q)$ is given by,

$$I_{gel}(q) = I_{Gel} \exp(-\frac{q^2 \Xi^2}{2}) \quad (3)$$

I_{Gel} is the scaling factor, which is related to the amount of the static heterogeneities. Ξ is the size of the static heterogeneities. This expression was frequently used to describe "frozen-in" crosslinks of gels.[38] Here, the gel term $I_{gel}(q)$ allows identifying the size and the amount of the static heterogeneities formed by physical crosslinks in PNIPMAM solutions, which give rise to the scattering at intermediate momentum transfers, $q \cong 0.1$ nm^{-1}.

The term $I_{fluct}(q)$ was applied to describe the chain scattering, indicating the correlation length caused by local concentration fluctuations, ξ_{OZ}, and the interactions between polymer chains and solvent molecules. A modified Ornstein-Zernike term was used:[39]

$$I_{fluct}(q) = \frac{I_{OZ}}{1+(q\xi_{OZ})^m} \quad (4)$$

with I_{OZ} the scaling factor. m is the Ornstein-Zernike exponent associated with the chain conformation, which is a result of the interactions between polymers and solvent molecules. For m = 2, the normal Ornstein-Zernike function is recovered, which describes polymer chains having

a Gaussian chain conformation.[40] $m > 2$ is obtained for a more compact local chain conformation due to a poorer solvent quality.

However, as the temperature increases in the one-phase state, the gel term $I_{gel}(q)$ at $q \cong 0.1$ nm^{-1} becomes less prominent and the forward scattering $I_{agg}(q)$ becomes much stronger, which makes it difficult to differentiate the two contributions. This was also the case for the 30 g L^{-1} PNIPMAM solution at all temperatures in the one-phase state. In these cases, the gel term was omitted from the model in eq 1 in these cases.

Eq 1 without the gel term was also used to analyze all SANS curves in the two-phase state. Here, the strong forward scattering in the low q region is mainly attributed to the formation of compact large aggregates (called mesoglobules).[5-9] The Porod exponent α of the modified Porod term $I_{agg}(q)$ describes their surface structure: $\alpha = 4$ is obtained for mesoglobules with smooth surfaces, $\alpha < 4$ for rough surfaces and $\alpha > 4$ for a concentration gradient near the mesoglobule surface.[41, 42] At all temperatures, the incoherent background I_{bkg} was kept fixed at values of 0.06 ± 0.01, 0.11 ± 0.01, and 0.13 ± 0.01 cm^{-1} for 30, 100, and 150 g L^{-1}, respectively.

Analysis of VSANS Curves. Only the VSANS curves of the 30 g L^{-1} PNIPMAM solution were analyzed, because the VSANS curves of the 100 and 150 g L^{-1} PNIPMAM solutions suffered from multiple scattering. For the 30 g L^{-1} PNIPMAM solution, only the VSANS curves above T_{CP} showed sufficient signal to be analyzed, and the Beaucage model was chosen:[43, 44]

$$I(q) = G\exp\left(-\frac{q^2 {R_g}^2}{3}\right) + B\left\{\left[\mathrm{erf}\left(\frac{qR_g}{\sqrt{6}}\right)\right]^3 / q\right\}^{\alpha'} + I_{bkg} \qquad (5)$$

It comprises the scaling factors G and B, the radius of gyration of the mesoglobules, R_g, the Porod exponent α' characterizing their surface roughness[41, 42] and the incoherent background I_{bkg} which

was fixed at 30 cm^{-1}. The error function erf(x) provides a smooth transition between the two contributions.

The invariant Q^*, used to estimate the water fraction in the polymer-rich domains, was calculated as follows:

$$Q^* = \int_0^\infty I(q) q^2 dq \quad (6)$$

where $I(q)$ is the scattered intensity. For a two-phase system, Q^* reads:

$$Q^* = 2\pi\phi(1-\phi)(\Delta\rho)^2 \quad (7)$$

where ϕ is the volume fraction of the polymer-rich domains and $\Delta\rho$ is the scattering length density difference between polymer-rich and solvent-rich domains. It was calculated over the entire q range from the fitted Beaucage model (eq 5) without the I_{bkg} term.

In the analysis of the SANS and the VSANS data, smearing effects owing to the wavelength spread and the divergence of the incident neutron beam were taken into account using standard procedures.[45] The SANS and VSANS curves were modeled using the SANS Data Reduction and Analysis software package 7.10 provided by the NIST Center for Neutron Research in the IGOR Pro software environment.[46]

3. Results and Discussion

This section is structured as follows: First, the overall phase behavior of aqueous PNIPMAM solutions, as determined by turbidimetry and optical microscopy, is described, and the thermal properties from DSC are presented. Secondly, the SANS and VSANS results are presented, giving insight into the temperature-dependent morphologies in a wide range of length scales. Thirdly, Raman spectroscopy unravels the dehydration behavior of the hydrophobic groups. Finally, all

results from PNIPMAM solutions are discussed and compared with PNIPAM solutions, before the manuscript is concluded.

a) Phase Behavior

The phase diagram of the PNIPMAM solutions in D_2O is established by determining the cloud points T_{CP} using turbidimetry in the concentration range 2-150 g L^{-1}. To avoid non-equilibrium states, a very low heating rate is chosen (0.2 K min^{-1}). The transmission curves are presented in Figure 1a. Below T_{CP}, the normalized transmission is constant at a value of one, i.e. the solutions are transparent. At T_{CP}, the transmission shows an abrupt drop, i.e. the solutions change from clear to turbid due to the formation of large mesoglobules. The transitions are all rather sharp, except for the solution with the lowest concentration (2 g L^{-1}), where the decay is broad, and the transmission above T_{CP} remains slightly above zero. The T_{CP} values lie in the range 42-45 °C (Figure 1b, Table 1) and decrease with increasing polymer concentration, as expected for LCST type polymers of rather low concentration. The values are in accordance with the ones reported in the literature (mostly 43 °C).[20, 22, 24] The fact that similar values are obtained by us confirms the type II behavior. Therefore, the relatively low molar mass (M_n^{app} = 17,000 g mol^{-1}) and rather high dispersity of our sample ($Đ$ = 1.74) does not seem to affect the cloud points notably.

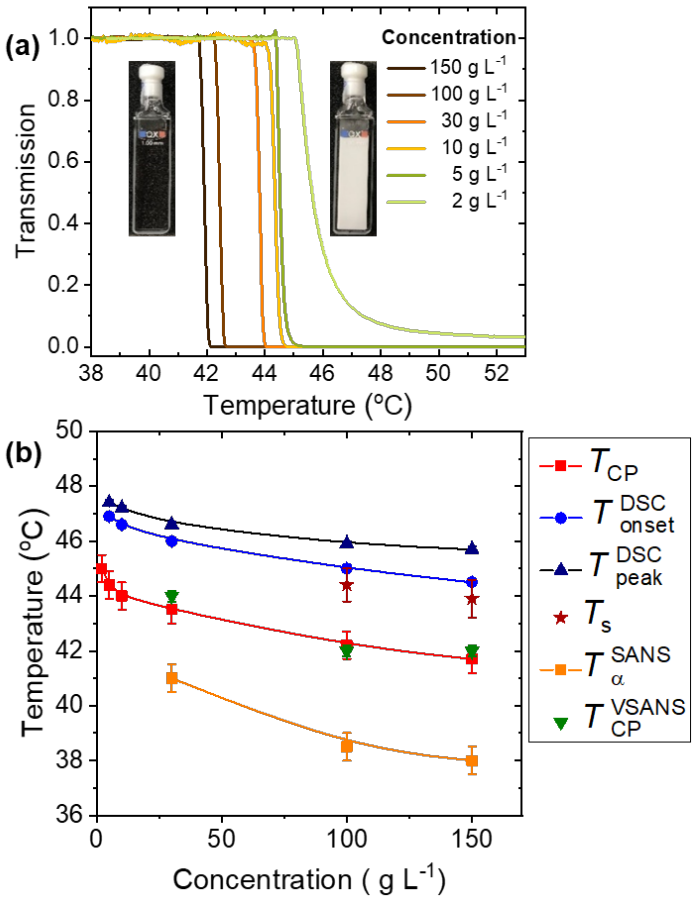

Figure 1. (a) Light transmission of PNIPMAM solutions in D_2O in dependence on temperature at a heating rate of 0.2 K min^{-1}. The concentrations are given in the graph. The photos show solutions of the 30 g L^{-1} solution below (left) and above the phase transition (right). (b) Cloud points determined by turbidimetry, onset and peak temperatures from DSC, spinodal temperatures T_s from the Ornstein-Zernike structure factor in SANS and the transition temperatures determined from the Porod exponent and from VSANS, as indicated in the graph.

Table 1. Results from turbidimetry, DSC and VSANS measurements

Concentrations (g L^{-1})	T_{CP} (°C)	T_{onset}^{DSC} (°C)	T_{peak}^{DSC} (°C)	ΔH (J/g_s)	T_{CP}^{VSANS}(°C)
2	45.0 ± 0.5	-	-	-	-
5	44.4 ± 0.5	46.9 ± 0.2	47.4 ± 0.1	0.17 ± 0.02	-
10	44.0 ± 0.5	46.6 ± 0.2	47.2 ± 0.1	0.39 ± 0.02	-
30	43.5 ± 0.5	46.0 ± 0.2	46.6 ± 0.1	1.29 ± 0.02	44.0 ± 1.0
100	42.2 ± 0.5	45.0 ± 0.2	45.9 ± 0.1	4.54 ± 0.02	42.0 ± 1.0
150	41.7 ± 0.5	44.5 ± 0.2	45.7 ± 0.1	6.40 ± 0.02	42.0± 1.0

b) Thermal Behavior

DSC measurements were carried out in the concentration range 5-150 g L^{-1}. Figure 2a shows the thermograms. Upon heating, the solutions undergo an endothermic transition at 45-47 °C, depending on concentration, as observed previously.[25, 47] The onset temperature and the peak temperature of the phase transition are given in Figure 1b and Table 1. Both decrease with increasing polymer concentration, as observed using turbidimetry. However, the onset temperature of the phase transition, related to the dehydration, is consistently 2-3 °C higher than T_{CP} from turbidimetry. Thus, upon heating, the PNIPMAM solutions first form large mesoglobules (at T_{CP} ≅ 42-45 °C), before the polymer chains dehydrate 2-3 °C above (at T_{onset}^{DSC} ≅ 45-47 °C). The peak areas provide the enthalpy of the phase transition, ΔH. The values increase linearly with polymer concentration (Figure 2b and Table 1), and reach 6.40 J g_s^{-1} for the highest concentration studied, 150 g L^{-1}. From the slope, the enthalpy of the polymer independent of concentration is derived as ΔH_p = 0.043 ± 0.006 J g_s^{-1}/g L^{-1}. In all likelihood, these findings are only marginally affected by the dispersity, if at all.

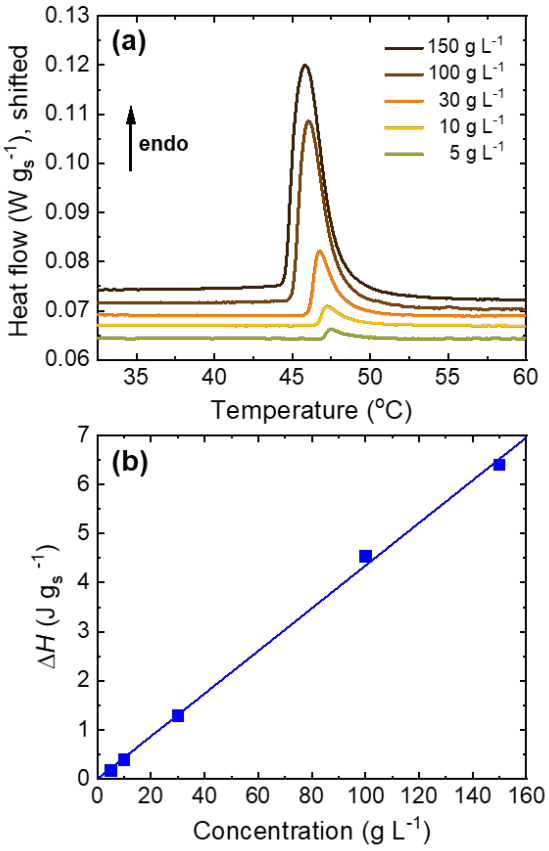

Figure 2. (a) DSC thermograms of PNIPMAM solutions in D_2O at a heating rate of 1 K min^{-1} at the concentrations given in the graph. For better visibility, the curves of 100 and 150 g L^{-1} are shifted vertically by 0.0030 and 0.0045, respectively. (b) Resulting concentration-dependent endothermic enthalpy ΔH (symbols). Line: linear fit.

c) Structural Properties Around the Cloud Point

Optical microscopy (OM) gives first insights into the phase-separated structures formed by PNIPMAM in aqueous solution. The OM images of a 150 g L^{-1} PNIPMAM solution in D_2O are shown in Figure 3. The solution is homogeneous and transparent below T_{CP} (Figure 3a), while

mesoglobules with diameters of ~2 μm form at T_{CP} (Figure 3b). With increasing temperature, the mesoglobules grow and form even larger mesoglobules (Figure 3c and d).

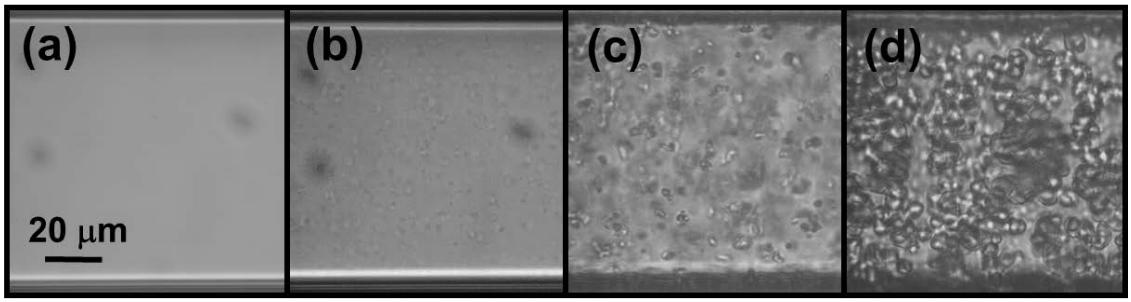

Figure 3. OM images of a 150 g L^{-1} PNIPMAM solution in D_2O below T_{CP} (a), at T_{CP} (b), just above T_{CP} (c), and far above T_{CP} (d). The dark spots in (a) and (b) are due to the background.

Small-Angle Neutron Scattering (SANS) is used to investigate the temperature-dependent mesoscopic structures of PNIPMAM in D_2O. These measurements enable us to probe the structures at length scales of ~1-100 nm, i.e. smaller structures than the ones resolved in OM. Representative SANS curves from solutions having concentrations of 30, 100 and 150 g L^{-1} are shown in Figure 4. Below T_{CP} (from turbidimetry), the scattering curves feature a decay at 0.03 – 0.06 nm^{-1} (called "forward scattering") and a shoulder at 0.2 – 2.0 nm^{-1} (called "chain scattering"). The intensity of the forward scattering increases with temperature. Thus, large-scale inhomogeneities are present already below T_{CP} and become more prominent as temperature is increased towards T_{CP}. The intensity of the chain scattering, which is caused by local concentration fluctuations in the semi-dilute polymer solutions, also increases, as T_{CP} is approached. Above T_{CP}, the intensity of the forward scattering is significantly higher, indicating the formation of mesoglobules. The intensity of the chain scattering decreases strongly with increasing temperature, suggesting that the contribution from large mesoglobules dominates.

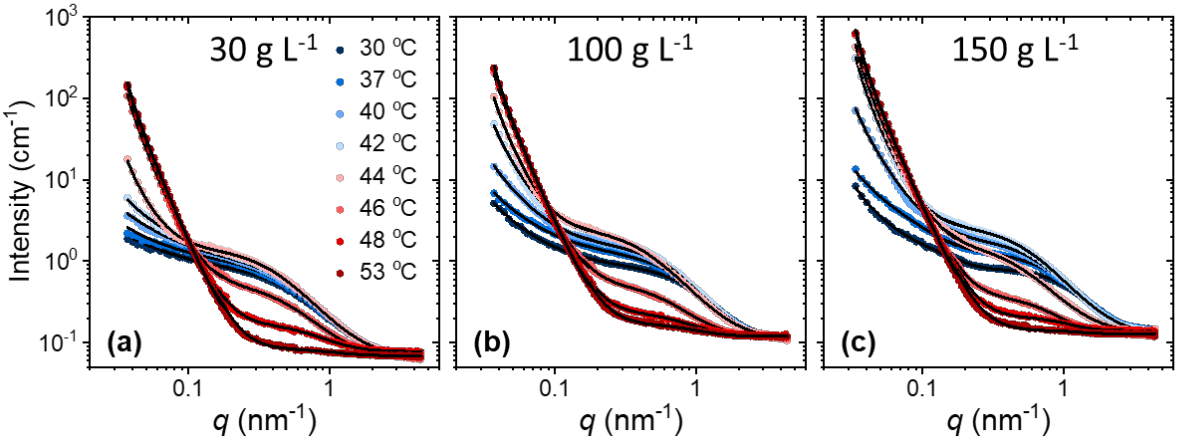

Figure 4. Representative SANS data of the (a) 30 g L^{-1}, (b) 100 g L^{-1}, and (c) 150 g L^{-1} PNIPMAM solutions in D_2O (symbols) at temperatures as given in (a). Blue and red color indicate temperatures below and above T_{CP} from turbidimetry, respectively. Black lines: fitting curves.

Usually, the scattering curves of semi-dilute polymer solutions in the one-phase state (e.g. from aqueous PNIPAM solutions) only feature chain scattering and very weak forward scattering. Thus, the scattering curves of PNIPAM solutions are typically well described by the (normal) Ornstein-Zernike model.[40, 48] However, the SANS curves from PNIPMAM solutions cannot be successfully modeled with this term alone, as demonstrated exemplarily in Figure S1 in the SI, in agreement with our previous results.[32] One reason is the forward scattering due to more pronounced large-scale inhomogeneities. Besides, for 100 and 150 g L^{-1} between 30 and 37 °C, there is an additional "bump" at $q \cong 0.1$ nm^{-1}, which is possibly caused by the structures resulting from physical crosslinks of the hydrophobic groups. Furthermore, the shape of the chain scattering at $q \cong 0.2 - 2.0$ nm^{-1} is different from the normal Ornstein-Zernike model. The negative slope of the decay is higher than 2 (Figure S1 in the SI), indicating a more compact local chain conformation, presumably due to attractive segment-segment interactions. Therefore, the model function given

in eq 1 is employed to analyze the SANS curves quantitatively in the one-phase state instead of the Ornstein-Zernike model. It features a modified Ornstein-Zernike term, which accounts for non-ideal chain conformations, a Porod term describing the forward scattering from large inhomogeneities, and a gel term describing the bump at $q \cong 0.1$ nm^{-1} due to physical crosslinks. Excellent fits are obtained (Figure 4), see the contributions and the full fit in Figure 5a and b. At temperatures just below T_{CP}, the amplitude of the gel term is negligible, and it is therefore omitted, i.e. eq 1 without the gel term is used instead. The same holds for all temperatures at 30 g L^{-1}.

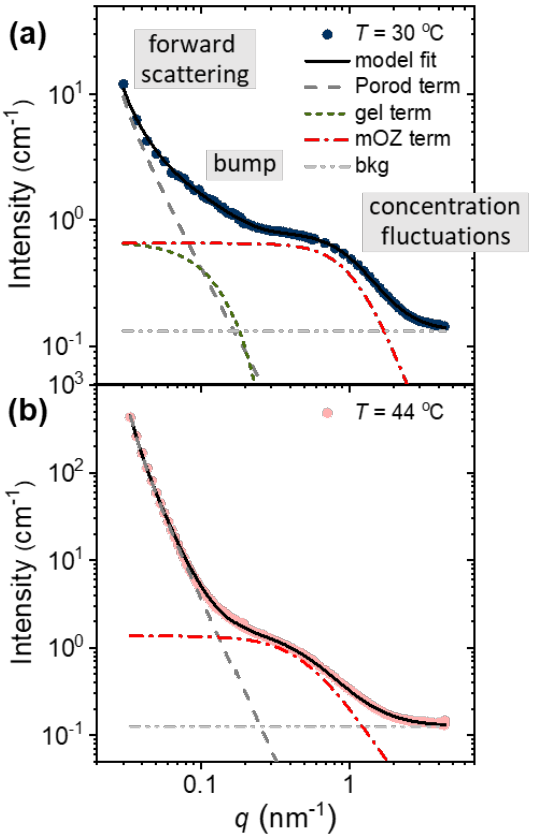

Figure 5. Representative SANS data of the 150 g L^{-1} PNIPMAM solutions in D_2O at (a) 30 °C, and (b) 44 °C (symbols). Full black lines: overall model fits. The other lines indicate the contributions to the models as described in the graphs. mOZ stands for modified Ornstein-Zernike model.

Similarly, for the scattering curves of polymer solutions in the two-phase state (e.g. from aqueous PNIPAM solutions), a model comprising the Porod law and the normal Ornstein-Zernike model is typically used to describe the scattering from large mesoglobules and from local concentration fluctuations, respectively.[40, 48] In PNIPMAM solutions, a similar model (eq 1 without the gel term) is applied to fit all the scattering curves in the two-phase state, namely the sum of the Porod term, and the modified Ornstein-Zernike term. Excellent fits are obtained in all cases (Figures 4 and 5b).

Regarding the temperature-dependent morphologies, the Ornstein-Zernike scaling factor I_{OZ} and correlation length ξ_{OZ} are shown in Figure 6a and b, respectively. In the one-phase state, both I_{OZ} and ξ_{OZ} increase as T_{CP} is approached and show the critical behavior expected for semi-dilute LCST-type polymer solutions with a divergence at the spinodal temperature T_s.[40] The values of the critical exponents γ and ν reflect the universality classes of the phase transitions and are determined by fitting the following power laws:

$$I_{OZ} \propto |T_s - T|^{-\gamma} \tag{9}$$

and

$$\xi_{oz} \propto |T_s - T|^{-\nu} \tag{10}$$

The fits are shown in Figure 6a and b and in double-logarithmic representation in Figure 6d and e. The resulting spinodal temperatures and the critical exponents are compiled in Table 2. For the 30 g L^{-1} PNIPMAM solution, I_{OZ} and ξ_{OZ} increase as well; however, we refrain from fitting eqs 9 and 10 due to a lack of data points.

For concentrations of 100 and 150 g L^{-1}, T_s values of ~44.5 °C are obtained both from I_{OZ} and ξ_{OZ} which is ~ 2 °C higher than T_{CP} from turbidimetry (Table 1). The critical exponents γ and ν

are ~0.7 and ~0.35, respectively. The Ornstein-Zernike exponent, *m*, which is related to the chain conformation and thus to the interactions between polymers and solvent molecules, is ~2.4-3.2 in the one-phase state for all concentrations studied (Figure 6c).

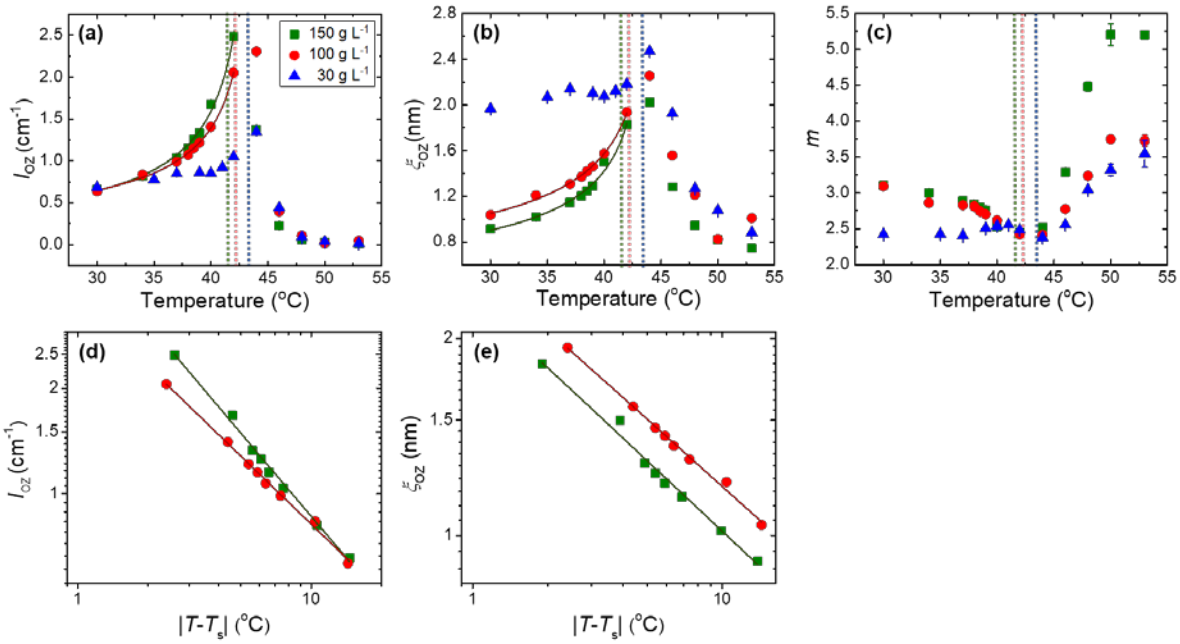

Figure 6. Structural parameters from model-fit results of the SANS data on the 30 (blue), 100 (red) and 150 g L^{-1} (green) solutions of PNIPMAM in D_2O in dependence on temperature, as indicated in (a). The dashed lines indicate the T_{CP} values from turbidimetry (same colors as the data). (a) Scaling factor of the mOZ term, I_{OZ}, (b) OZ correlation length ξ_{OZ}, and (c) OZ exponent *m*. Double-logarithmic representation of I_{OZ} (d) and ξ_{OZ} (e) in dependence on the absolute difference to the spinodal temperature T_s. The solid lines are fits to the data.

Table 2. Characteristic temperatures and critical exponents determined from SANS measurements on PNIPMAM solutions in D_2O

Concentration (g L^{-1})	T_s (°C) from I_{OZ}	γ	T_s (°C) from ξ_{OZ}	ν
100	44.4 ± 0.4	0.64 ± 0.06	44.4 ± 0.6	0.34 ± 0.04
150	44.6 ± 0.6	0.78 ± 0.10	43.9 ± 0.7	0.36 ± 0.06

Upon heating through T_{CP}, both I_{OZ} and ξ_{OZ} decrease drastically in accordance with the collapse of the polymer chains. *m* increases significantly with temperature to values far higher than in the one-phase state. This indicates that, in the two-phase state, the attractive segment-segment interactions become even stronger, which results in much more compact chain conformations. However, local concentration fluctuations are still present.

The scaling factor of the gel term I_{Gel} and the size of the static heterogeneities Ξ are shown in Figure 7a and b. They are attributed to the number density and the size of the static heterogeneities formed by physical crosslinks caused by the hydrophobic groups in PNIPMAM, respectively. At 30 °C, Ξ is ~4 nm and ~10 nm for 100 and 150 g L^{-1}, respectively. For 100 g L^{-1}, Ξ and I_{Gel} are weakly changing with temperature. For 150 g L^{-1}, both Ξ and I_{Gel} increase notably when T_{CP} is approached, meaning that the static heterogeneities composed of physical crosslinks become larger and more prominent. This may be attributed to an increase of concentration fluctuations close to T_{CP} and the stronger segment-segment interactions. The number density and the size of the static heterogeneities comprising physical crosslinks increase with polymer concentration. Above 38 °C, the forward scattering caused by the large-scale inhomogeneities becomes so pronounced, that further characterization of the static heterogeneities is no longer possible.

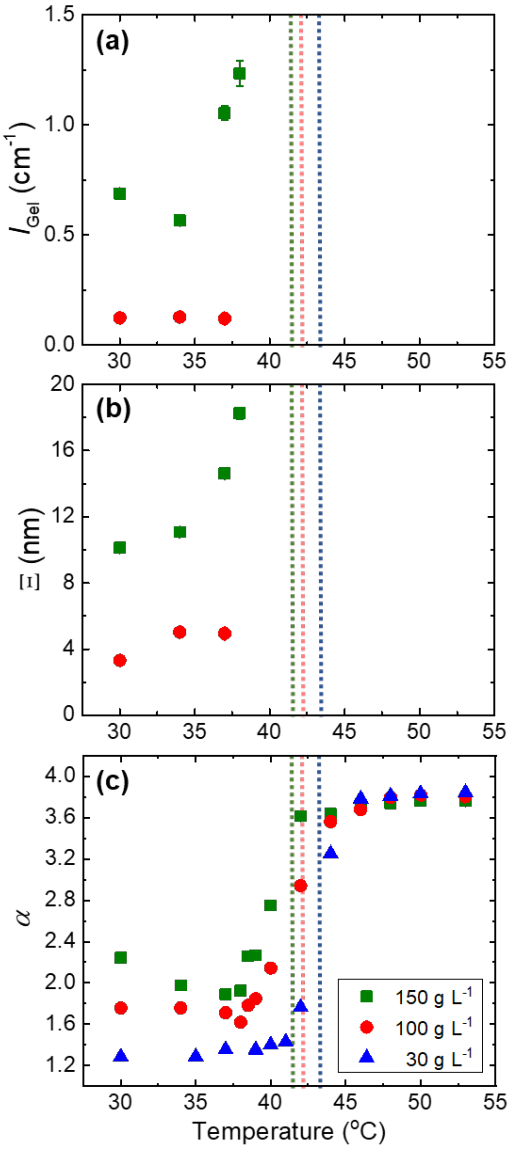

Figure 7. Structural parameters from model-fit results of the SANS data on the 30 (blue), 100 (red) and 150 g L^{-1} (green) PNIPMAM solutions in D_2O in dependence on temperature, as indicated in (c). The dashed lines indicate the T_{CP} values from turbidimetry (same colors as the data). (a) Scaling factor of physical crosslinks I_{Gel}, (b) correlation length of physical crosslinks Ξ, and (c) Porod exponent α.

The Porod exponent α is shown in Figure 7c. For 150 g L^{-1}, α is ~2 below T_{CP} (at 30-38 °C), i.e. the large-scale inhomogeneities are loose fractals.[37] A few degrees below T_{CP} (at 38-42 °C), α abruptly increases to 3.6, meaning that they become compact. A transition temperature T_α^{SANS} can be identified from the onset of the increase of α. For all concentrations, T_α^{SANS} is 2.5-3 °C below the T_{CP} determined by turbidimetry; thus, structural changes on the mesoscopic length scale occur consistently ~3 °C below T_{CP}. Above T_{CP}, α describes the surface structure of the mesoglobules. For all concentrations, α stays constant at ~3.8 above T_{CP}, meaning that large mesoglobules with rather smooth surfaces are formed by the collapsed polymer chains.

Regarding the concentration-dependent morphologies, in general, ξ_{OZ} decreases and I_{OZ} increases with increasing polymer concentration in the one-phase state. In the two-phase state, ξ_{OZ} and I_{OZ} are hardly concentration-dependent (Figure 6a and b). m increases with increasing concentration. Regarding the static heterogeneities, we find that Ξ is 10-18 nm for 150 g L^{-1}, but only 4-5 nm for 100 g L^{-1}. I_{gel} is ~0.75-1.25 cm^{-1} for 150 g L^{-1} and thus higher than for 100 g L^{-1} (~0.12 cm^{-1}, Figure 7a and b). Thus, the static heterogeneities formed by physical crosslinks are smaller and less abundant at lower concentration, as expected. At the lowest concentration, i.e. at 30 g L^{-1}, they are not observed. Regarding the large-scale inhomogeneities in the one-phase state, we find that α increases with concentration, i.e. large-scale inhomogeneities are more loosely packed when the polymer solutions are more dilute. In the two-phase state, the surface of the large mesoglobules is rather smooth independent of the concentration. Furthermore, the phase transition temperature T_α^{SANS} decreases with increasing concentration.

Very Small-Angle Neutron Scattering (VSANS) is used to characterize the size and water content of the mesoglobules. Representative data of the 30 g L^{-1} PNIPMAM solution in D_2O are displayed in Figure 8a along with the SANS results discussed above (also in Figure S4a).

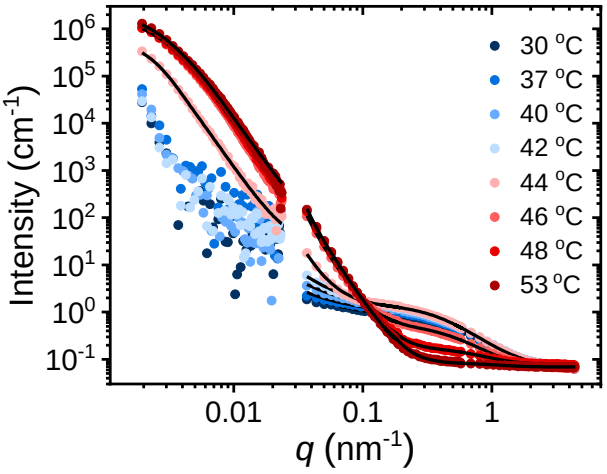

Figure 8. Representative VSANS and SANS data of the 30 g L^{-1} PNIPMAM solution in D_2O (symbols). Full black lines: model fits.

During the VSANS measurements, the neutron transmission was measured at all temperatures. The temperature at which it starts to decay drastically (Figure S2 in the SI), was identified as T_{CP}^{VSANS}. For the 30 g L^{-1} PNIPMAM solution, T_{CP}^{VSANS} is 44.0 ± 1.0 °C (Table 1), which is in accordance with the T_{CP} value determined by turbidimetry (43.5 ± 0.5 °C).

At 100 and 150 g L^{-1}, the transmission is below 0.7 in the one-phase state and below 0.05 in the two-phase state. This indicates significant multiple scattering, hampering further analysis (see Figure S2 in the SI). Therefore, only the data at 30 g L^{-1} are evaluated quantitatively.

Below T_{CP}^{VSANS}, the VSANS curves feature a decay, confirming the presence of large-scale inhomogeneities already in the one-phase state. Above T_{CP}^{VSANS}, the shape of the VSANS curves turns into a pronounced shoulder of much higher intensity, indicating the formation of compact mesoglobules.

Since the intensities of the VSANS curves at temperatures below T_{CP}^{VSANS} are rather noisy, they are not analyzed by fitting structural models. Above T_{CP}^{VSANS}, the Beaucage model was used,

which provides information on the size and the surface roughness. The invariant Q^* indicates the water content of the mesoglobules. The contributions to the Beaucage model are shown exemplarily in Figure S3 in the SI. Excellent fits are obtained at all temperatures above T_{CP}^{VSANS} (Figure 8).

The radius of gyration R_g of the mesoglobules is displayed in Figure 9a. For the 30 g L^{-1} PNIPMAM solution, R_g is ~910-960 nm at 44 and 45 °C and ~750 nm at 46 °C and above. The overall decrease upon heating is attributed to the release of water. The Porod exponent α' is ~3.9 at all temperatures, i.e. the surface of the mesoglobules is rather smooth (see also Figure S6a in the SI), in accordance with the results for α from SANS (Figure 7c). The invariant Q^* (eq 6), calculated from the fitted Beaucage functions, is related to the fraction of D_2O in the PNIPMAM-rich mesoglobules (eq 7, Figure 9b). Q^* increases abruptly at T_{CP}^{VSANS} and remains constant above ~T_{CP}^{VSANS} + 1 °C, revealing the dehydration of the mesoglobules, which enhances the scattering contrast.

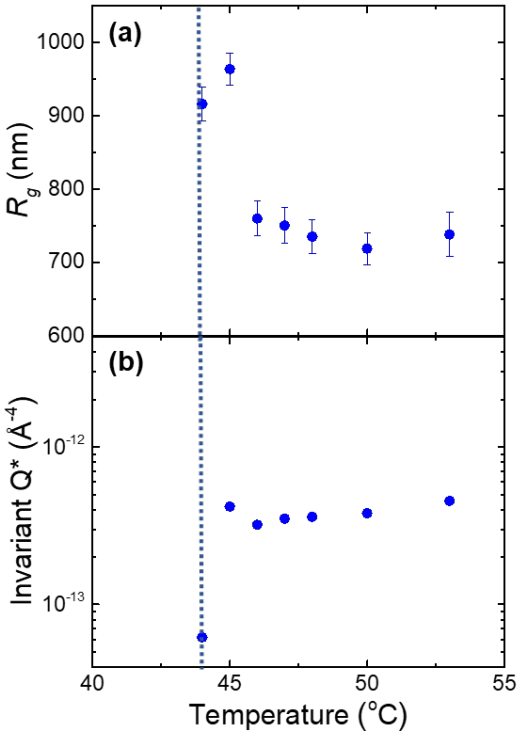

Figure 9. (a) Radius of gyration of the mesoglobules R_g and (b) invariant Q^* of the 30 g L^{-1} PNIPMAM solution in D_2O, determined by VSANS. Dashed line: T_{CP}^{VSANS}.

To reduce multiple scattering from PNIPMAM solutions at 100 and 150 g L^{-1}, the VSANS measurements are performed not only in D_2O (Figure S4 in the SI), but also in 50:50 v/v mixtures of D_2O and H_2O (Figure S5 in the SI). The neutron transmission values are ~0.58 in the one-phase state and ~0.18-0.25 in the two-phase state (Figure S2 in the SI). These values above T_{CP}^{VSANS} are still too low to enable to a reliable analysis of the data. Only at 44 °C, where the neutron transmissions are still higher than 0.5, the radius of gyration of the mesoglobules may be estimated at ~1.1 μm and 1.0 μm for the 100 and 150 g L^{-1}, respectively (see Figure S5 in the SI). These values are slightly larger than the ones from the 30 g L^{-1} PNIPMAM solution in pure D_2O.

d) Dehydration Behavior of the Hydrophobic Groups

For PNIPAM, the hydrophilic amide groups remain hydrated even above the transition temperature, while the hydrophobic interactions play a dominant role for the phase transition,[49-51] and the vibrational frequencies of the hydrophobic groups are sensitive to hydration.[16, 28, 49, 50] To characterize the dehydration behavior of the hydrophobic groups in PNIPMAM solutions, we performed temperature-dependent Raman spectroscopy around T_{CP} in the CH-stretching vibration region at a polymer concentration of 150 g L^{-1} in D_2O, as in SANS. The Raman spectra of the CH-stretching region of PNIPMAM around 2950 cm^{-1} are shown in Figure 10. Vibrational modes are detected at 2884, 2922, 2948, and 2991 cm^{-1} are attributed to symmetric stretching of the CH_3 groups, $\nu_s(CH_3)$, symmetric stretching of the CH groups, $\nu_s(CH)$, antisymmetric stretching of the CH_2 groups, $\nu_{as}(CH_2)$, and antisymmetric stretching of the CH_3 groups, $\nu_{as}(CH_3)$.[16, 28, 52] Above T_{CP}, all bands shift to lower frequencies.

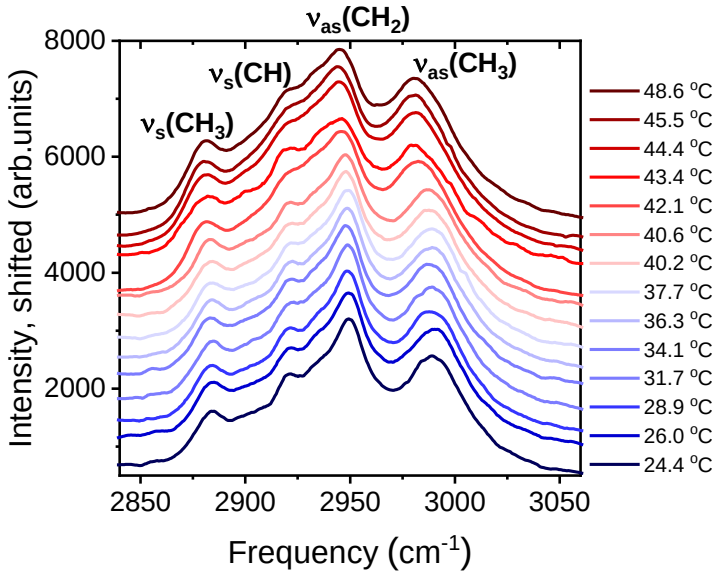

Figure 10. Raman spectra of the 150 g L^{-1} PNIPMAM solution in D_2O in dependence on temperature. Temperatures are given in the graphs. T_{CP} is determined at 39.0 °C by in situ optical

microscopy. Blue lines: below T_{CP}, red lines: above T_{CP}. For clarity, the spectra were smoothed by the Savitzky-Golay algorithm and are shifted vertically.

For a quantitative description of the peak frequencies, the CH-stretch spectral bands in the frequency range from 2850 to 3100 cm^{-1} are fitted using a superposition of four Lorentzian lineshapes. A small background due to the tail of the OD vibrational bands between 2200 and 2800 cm^{-1} is accounted for, as shown in Figure S7 in the SI. Figure S8 shows the deconvolution in the CH-stretching region. The peak frequencies of these four contributions are displayed in dependence on temperature in Figure 11. Below T_{CP}, they are constant, while, above T_{CP}, they decrease steadily. This means that the interactions between the hydrophobic substituents of PNIPMAM and D_2O molecules change, as T_{CP} is crossed. In other words, an abrupt red-shift occurs in the two-phase region, especially for the bands related to CH_3, as observed for PNIPAM.[16, 49] Accordingly, the hydrophobic substituents of PNIPMAM undergo a strong dehydration at T_{CP} and the hydrophobic interactions dominate during the phase transition. Moreover, upon heating, the full widths at half maximum of the Lorentzian functions of $\nu_s(CH)$ and $\nu_{as}(CH_3)$ increase significantly, and the one of $\nu_{as}(CH_2)$ increases gradually (Figure S9 in the SI). This indicates that, in the two-phase state, the molecular interactions around the CH groups become more disordered and inhomogeneous.

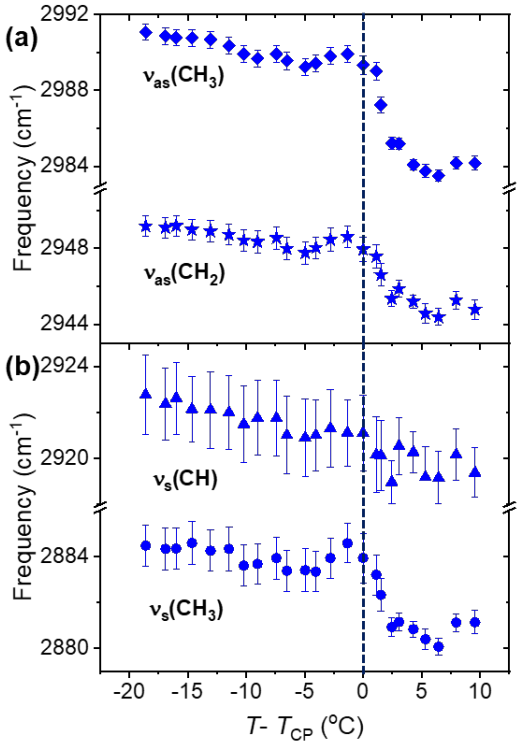

Figure 11. Results from Raman spectroscopy on the 150 g L^{-1} PNIPMAM solution in D_2O. Peak frequencies of (a) antisymmetric CH_3 ($\nu_{as}(CH_3)$), and antisymmetric CH_2 ($\nu_{as}(CH_2)$), and (b) symmetric CH ($\nu_s(CH)$), and symmetric CH_3 ($\nu_s(CH_3)$) stretching bands, as indicated in the graphs, in dependence on the temperature difference to T_{CP} from optical microscopy.

e) Comparison between aqueous PNIPAM and PNIPMAM solutions.

To understand how the additional methyl groups in PNIPMAM influence the phase behavior, thermal behavior, hydration behavior of the hydrophobic groups, and structural changes at the phase transition, we compare our results from aqueous PNIPMAM solutions with those of the analogous polyacrylamide PNIPAM. Both polymers exhibit type II LCST behavior. Accordingly, the results from the PNIPMAM solutions are barely influenced by its dispersity index (here: $Đ$ = 1.74).

Turbidimetry and DSC show that PNIPMAM solutions undergo the phase transition at higher temperature ($T_{CP} \cong 43$ °C) than PNIPAM ($T_{CP} \cong 32$ °C). Furthermore, they reveal that T_{onset}^{DSC} is 2-3 °C higher than T_{CP} in the case of PNIPMAM, indicating that mesoglobules are formed before the polymer chains dehydrate. In aqueous PNIPAM solutions, T_{CP} and T_{onset}^{DSC} are equal within the uncertainties (0.5 °C), see Figure S10 and Table S1 in the SI. This indicates that, in the PNIPAM solutions, the formation of large mesoglobules and the dehydration occur simultaneously upon heating. Thus, PNIPMAM solutions not only undergo the phase transition at higher temperatures, but also feature a more complex phase transition process than PNIPAM.

Additionally, the value of the enthalpy of the polymer independent of concentration, ΔH_p, has a value of 0.043 ± 0.006 J g_s^{-1}/g L^{-1} for the PNIPMAM solutions which is higher than for PNIPAM ($\Delta H_p = 0.031 \pm 0.003$ J g_s^{-1}/g L^{-1}, Figure S11b in the SI). This difference is in accordance with the findings in ref. 24. In PNIPAM solutions, the hydrophilic amide groups mostly remain hydrated and the hydrophobic interactions dominate.[49-51] Therefore, the endothermic heat during the phase transition is mainly due to the hydrophobic dehydration. As PNIPMAM has more hydrophobic groups, its enthalpy change at the phase transition is larger than the one from PNIPAM.

The critical behavior when approaching the phase transition differs as well. In the one-phase state, the critical exponents ν and γ of the PNIPMAM solutions are ca. 0.35 and 0.7 and thus significantly smaller than the values predicted by mean-field theory ($\nu = 0.5$ and $\gamma = 1.0$).[53, 54] The deviation may be due to the fact that the phase transition of PNIPMAM is not of first or of higher order. For a purely first-order phase transition, the critical behavior is absent.[55] Though less pronounced values lower than the mean-field ones were reported also for aqueous PNIPAM solutions, namely $\nu = 0.44 \pm 0.01$ and $\gamma = 0.81 \pm 0.01$,[48] it was doubted that this was due to the higher order of the phase transition.[56, 57] A more likely reason may be the long-range concentration

fluctuations observed for both polymers which are significantly more pronounced in the PNIPMAM solutions. Furthermore, the segment-segment interactions in the PNIPMAM solutions are enhanced and the chain conformation is more compact, as evidenced by the high values of the Ornstein-Zernike exponent m compared to the values $m = 2$ found previously for PNIPAM.[40, 48] We ascribe this difference to the additional hydrophobic methyl groups in PNIPMAM.

Overall, three main morphological differences emerge between PNIPMAM and PNIPAM in aqueous solution. Firstly, in the one-phase state, loosely packed large-scale inhomogeneities are much more pronounced for PNIPMAM. Secondly, physical crosslinks give rise to inhomogeneities at intermediate length scales. Thirdly, the chain conformation of PNIPMAM in aqueous solutions below T_{CP} is more compact. All these observations are mainly a consequence of the enhanced attractive segment-segment interactions between the hydrophobic moieties already in the one-phase state.

OM and VSANS revealed size differences of the mesoglobules from PNIPMAM and PNIPAM solutions above T_{CP}. Comparing the VSANS results of the 30 g L^{-1} PNIPMAM solution (which corresponds to 2.7 wt%) with the ones of a 3 wt% PNIPAM solution, which was measured previously at the same instrument (Figure S6 in the SI),[9] it is seen that the R_g values of the mesoglobules formed by PNIPMAM are consistently larger than the ones from PNIPAM, namely by a factor of ~2-3. Furthermore, the invariant Q^* from PNIPMAM is almost 2 orders of magnitude smaller than the one from PNIPAM, reflecting that the mesoglobules from PNIPMAM contain more D_2O than the ones from PNIPAM. These findings may be attributed to the steric hindrance induced by the additional methyl groups on the polymer backbone, hampering a dense packing.

The difference of the hydration behavior of the hydrophobic groups between PNIPMAM and PNIPAM solutions can be determined by comparing the results from Raman spectroscopy with

the ones from a 3 wt% PNIPAM solution in D_2O measured with the same setup and analyzed with the same method (Figure S12 in the SI).[9] In the one-phase state, the peak frequency of $\nu_{as}(CH_3)$ from PNIPMAM is ~2991 cm^{-1}, while it is ~2989 cm^{-1} for PNIPAM. A similar shift is observed for $\nu_{as}(CH_2)$ and $\nu_s(CH_3)$, but not for $\nu_s(CH)$. Higher peak frequencies suggest that the hydrophobic groups of PNIPMAM are more hydrated than the ones of PNIPAM (Figure S12). Previous experiments with infrared spectroscopy addressed the hydration behavior of the hydrophilic amide groups of PNIPMAM and of PNIPAM via the frequency of the amide II band.[28] In the one-phase state, the peak frequency of the amide II groups for PNIPMAM is ~1538 cm^{-1}, whereas the one of PNIPAM is ~1562 cm^{-1}. Accordingly, the amide groups of PNIPMAM are less hydrated than the ones of PNIPAM. Thus, the hydrophobic groups of PNIPMAM are surrounded by more water molecules, while the hydrophilic amide groups are surrounded by less water molecules (Figure S13 in the SI). This may be attributed to steric hindrances caused by additional methyl groups in PNIPMAM. However, in interpreting these differences, one should keep in mind that the PNIPMAM and PNIPAM samples studied here and in ref. 9 differ in molar mass (M_n = 17,000 g/mol and 36,000 g/mol, respectively). Computer simulations for PNIPAM suggest that the degree of hydration of the polymer chain decreases with increasing molar mass.[58] Still, this effect levels off for polymers with degrees of polymerization above 30 and is presumably negligible for the polymers discussed here, $PNIPAM_{319}$ and $PNIPMAM_{133}$.[58]

In the two-phase state, the peak frequency of all CH-stretching bands of PNIPMAM and PNIPAM are shifted to lower wavenumbers, showing that the dehydrated state of the hydrophobic groups from the collapsed PNIPMAM and PNIPAM chains is similar. As for the $\nu_{as}(CH_3)$ band, this is consistent with the infrared spectroscopy results on the $\nu_{as}(CH_3)$ in the two-phase state.[28] Moreover, the infrared spectroscopy results on the amide II band in ref. 28 indicate that, in the

two-phase state, the intermolecular interactions between the amide groups of PNIPMAM are weaker than the ones of PNIPAM. This weakening may be attributed to the steric hindrances caused by the presence of the methyl groups. Moreover, it is consistent with the higher water content and larger size of the mesoglobules formed by PNIPMAM found using VSANS.

To summarize, PNIPMAM solutions feature not only higher phase transition temperatures but also a more complex phase transition process. The additional methyl groups change hydration behavior of the hydrophobic groups from PNIPMAM in the one-phase state. The structural behavior of PNIPMAM and PNIPAM in D_2O around the cloud point is summarized in Figure 12. In the one-phase state, loosely packed large-scale inhomogeneities and physical crosslinks caused by hydrophobic groups are present in the PNIPMAM solution. Furthermore, the local chain conformation of PNIPMAM is more compact than the one of PNIPAM, which is attributed to the hydrophobic effect and enhanced attractive segment-segment interactions induced by the additional methyl groups. In the two-phase state, the chains are collapsed and mesoglobules form, which shrink with increasing temperature. The mesoglobules formed by PNIPMAM are larger and contain more water than the ones of PNIPAM at a similar polymer concentration.

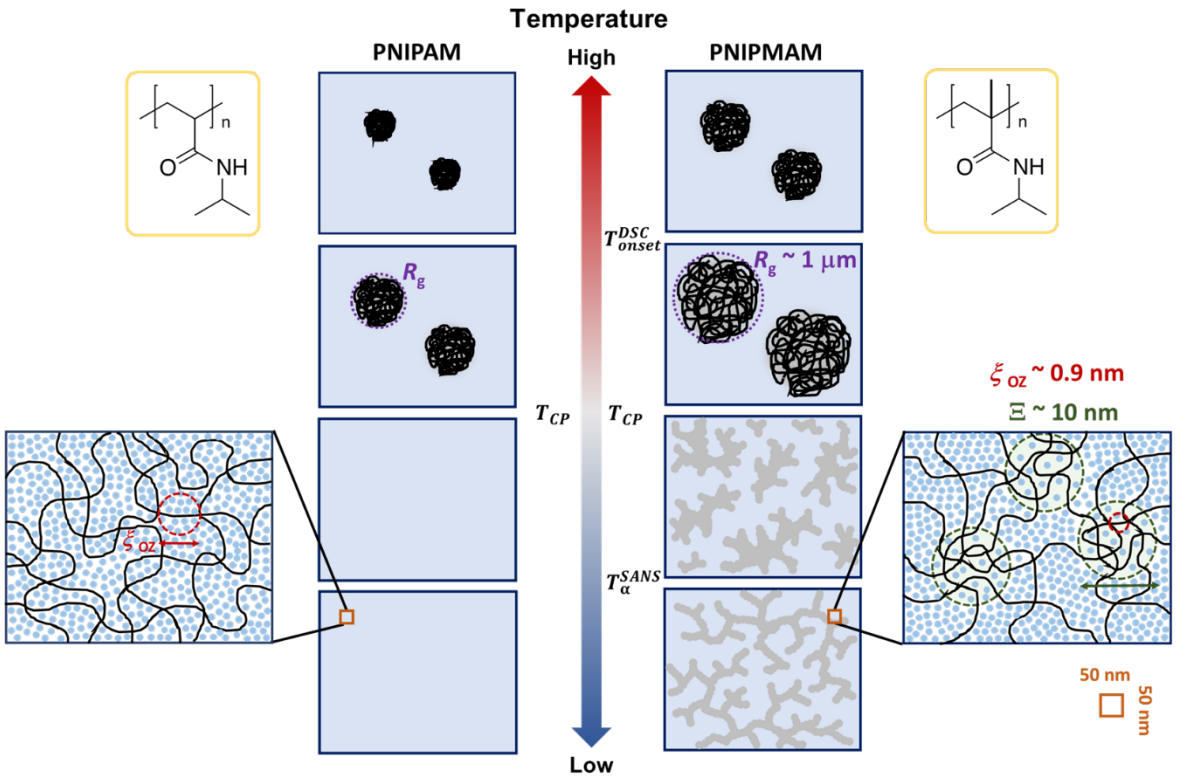

Figure 12. Schematic structures of PNIPAM and PNIPMAM in D_2O in dependence on temperature. The polymers are shown as black lines, and the water molecules as light blue dots. The red circles mark the correlation length ξ_{OZ}, the green circles display the size of the physical crosslinks Ξ, and the purple circles illustrate the radius of gyration of the mesoglobules R_g. Characteristic length scales are indicated. The grey regions represent the large-scale inhomogeneities. The chemical structures are shown in the yellow boxes.

4. Conclusion

The present work addresses the phase transition mechanism of the thermoresponsive polymer PNIPMAM in aqueous solution. The phase diagram is constructed from results of turbidimetry and DSC measurements, revealing that the PNIPMAM chains dehydrate only 2~3 °C above T_{CP}, where macroscopic phase separation sets in. This is in contrast to the behavior of PNIPAM, for

which the turbidity and DSC transitions virtually coincide. From Raman spectroscopy, it is concluded that, compared to PNIPAM, the hydration behavior of the hydrophobic groups from PNIPMAM in the one-phase state is altered due to the steric hindrances caused by the additional methyl groups. SANS and VSANS results provide structural information of the temperature-dependent phase transition mechanism of aqueous PNIPMAM solutions. In the one-phase state, loosely packed large-scale inhomogeneities and the static heterogeneities formed by physical crosslinks are observed, which can be attributed to hydrophobic moieties induced by the additional methyl groups. These hydrophobic methyl groups also give rise to more compact local chain conformations in the one-phase state. The PNIPMAM chains collapse in the two-phase state, as expected for thermoresponsive polymers. Mesoglobules form and shrink with increasing temperature. The mesoglobules formed by PNIPMAM are larger and contain more water inside than the ones from PNIPAM. To conclude, the presence of a single additional methyl group in the backbone segment of the PNIPMAM chain leads to substantially different hydration and structural behavior around the phase transition, which explains the counter-intuitive shift of the transition to higher temperatures.

ASSOCIATED CONTENT

Supporting Information. The Supporting Information is available free of charge on the ACS Publications website at DOI: xxx.

Choice of fit model. Results from VSANS. Results from Raman spectroscopy. Turbidimetry and DSC measurements on PNIPAM solutions. Comparison of PNIPMAM with PNIPAM solutions. Cloud points.

AUTHOR INFORMATION

Corresponding Author

*Christine M. Papadakis, papadakis@tum.de

Author Contributions

The manuscript was written through contributions of all authors. All authors have given approval to the final version of the manuscript.

Funding Sources

We thank Deutsche Forschungsgemeinschaft (DFG) for financial support (PA 771/20-1, MU 1487/29-1, LA 611/16-1). A. S. acknowledges support by an August-Wilhelm Scheer visiting professorship at TU Munich.

ACKNOWLEDGMENT

We thank K. Shehu (TU München) for help with the SANS experiments, and S. Prentzel (Universität Potsdam) for support with the SEC measurements. This work is based upon experiments performed at the KWS-1 and KWS-3 instruments operated by JCNS at the Heinz Maier-Leibnitz Zentrum (MLZ), Garching, Germany. MLZ is acknowledged for beam time allocation and for providing excellent equipment.

REFERENCES

1. Islam, M. R.; Ahiabu, A.; Li, X.; Serpe, M. J. Poly (*N*-isopropylacrylamide) Microgel-Based Optical Devices for Sensing and Biosensing. *Sensors-Basel* **2014,** *14*, 8984-8995.

2. Sun, X.-L.; Tsai, P.-C.; Bhat, R.; Bonder, E. M.; Michniak-Kohn, B.; Pietrangelo, A. Thermoresponsive Block Copolymer Micelles with Tunable Pyrrolidone-Based Polymer Cores: structure/Property Correlations and Application as Drug Carriers. *J. Mater. Chem. B* **2015,** *3*, 814-823.

3. Tokarev, I.; Minko, S. Stimuli-Responsive Hydrogel Thin Films. *Soft Matter* **2009,** *5*, 511-524.

4. Pamies, R.; Zhu, K.; Kjøniksen, A. L.; Nyström, B. Thermal Response of Low Molecular Weight Poly-(*N*-isopropylacrylamide) Polymers in Aqueous Solution. *Polym. Bull.* **2009,** *62*, 487-502.

5. Halperin, A.; Kröger, M.; Winnik, F. M. Poly(*N*-isopropylacrylamide) Phase Diagrams: Fifty Years of Research. *Angew. Chem. Int. Ed.* **2015,** *54*, 15342-15367.

6. Gorelov, A. V.; Du Chesne, A.; Dawson, K. A. Phase Separation in Dilute Solutions of Poly (*N*-isopropylacrylamide). *Physica A* **1997,** *240*, 443-452.

7. Aseyev, V.; Hietala, S.; Laukkanen, A.; Nuopponen, M.; Confortini, O.; Du Prez, F. E.; Tenhu, H. Mesoglobules of Thermoresponsive Polymers in Dilute Aqueous Solutions above the LCST. *Polymer* **2005,** *46*, 7118-7131.

8. Balu, C.; Delsanti, M.; Guenoun, P.; Monti, F.; Cloitre, M. Colloidal Phase Separation of Concentrated PNIPAm Solutions. *Langmuir* **2007,** *23*, 2404-2407.

9. Niebuur, B.-J.; Claude, K.-L.; Pinzek, S.; Cariker, C.; Raftopoulos, K. N.; Pipich, V.; Appavou, M. S.; Schulte, A.; Papadakis, C. M. Pressure-Dependence of Poly(*N*-

isopropylacrylamide) Mesoglobule Formation in Aqueous Solution. *ACS Macro Lett.* **2017,** *6*, 1180-1185.

10. Tanaka, H. Appearance of a Moving Droplet Phase and Unusual Network-Like or Sponge-Like Patterns in a Phase-Separating Polymer-Solution with a Double-Well-Shaped Phase-Diagram. *Macromolecules* **1992,** *25*, 6377-6380.

11. Wu, C.; Li, W.; Zhu, X. X. Viscoelastic Effect on the Formation of Mesoglobular Phase in Dilute Solutions. *Macromolecules* **2004,** *37*, 4989-4992.

12. Tanaka, H. Viscoelastic Phase Separation. *J. Phys. Condens. Mat.* **2000,** *12*, R207-R264.

13. Terada, T.; Inaba, T.; Kitano, H.; Maeda, Y.; Tsukida, N. Raman-Spectroscopic Study on Water in Aqueous-Solutions of Temperature-Responsive Polymers - Poly(*N*-Isopropylacrylamide) and Poly[*N*-(3-Ethoxypropyl)Acrylamide]. *Macromol. Chem. Phys.* **1994,** *195*, 3261-3270.

14. Lin, S.-Y.; Chen, K.-S.; Liang, R.-C. Thermal Micro ATR/FT-IR Spectroscopic System for Quantitative Study of the Molecular Structure of Poly(*N*-isopropylacrylamide) in Water. *Polymer* **1999,** *40*, 2619-2624.

15. Katsumoto, Y.; Tanaka, T.; Sato, H.; Ozaki, Y. Conformational Change of Poly(*N*-isopropylacrylamide) during the Coil-Globule Transition Investigated by Attenuated Total Reflection/Infrared Spectroscopy and Density Functional Theory Calculation. *J. Phys. Chem. A* **2002,** *106*, 3429-3435.

16. Futscher, M. H.; Philipp, M.; Müller-Buschbaum, P.; Schulte, A. The Role of Backbone Hydration of Poly(*N*-isopropyl acrylamide) Across the Volume Phase Transition Compared to its Monomer. *Sci. Rep.* **2017,** *7*, 17012.

17. Schild, H. G. Poly (*N*-Isopropylacrylamide) - Experiment, Theory and Application. *Prog. Polym. Sci.* **1992,** *17*, 163-249.

18. Kojima, H.; Tanaka, F. Cooperative Hydration Induces Discontinuous Volume Phase Transition of Cross-Linked Poly(*N*-isopropylacrylamide) Gels in Water. *Macromolecules* **2010,** *43*, 5103-5113.

19. Aseyev, V.; Tenhu, H.; Winnik, F. M. Non-ionic Thermoresponsive Polymers in Water. *Adv. Polym. Sci.* **2011,** *242*, 29-89.

20. Fujishige, S.; Kubota, K.; Ando, I. Phase-Transition of Aqueous-Solutions of Poly(*N*-isopropylacrylamide) and Poly(*N*-isopropylmethacrylamide). *J. Phys. Chem.* **1989,** *93*, 3311-3313.

21. Chytrý, V.; Netopilík, M.; Bohdanecký, M.; Ulbrich, K. Phase Transition Parameters of Potential Thermosensitive Drug Release Systems Based on Polymers of *N*-alkylmethacrylamides. *J. Biomat. Sci-Polym. Ed.* **1997,** *8*, 817-824.

22. Netopilík, M.; Bohdanecký, M.; Chytrý, V.; Ulbrich, K. Cloud Point of Poly(*N*-isopropylmethacrylamide) Solutions in Water: Is It Really a Point? *Macromol. Rapid. Comm.* **1997,** *18*, 107-111.

23. Djokpé, E.; Vogt, W. *N*-isopropylacrylamide and *N*-isopropylmethacrylamide: Cloud Points of Mixtures and Copolymers. *Macromol. Chem. Phys.* **2001,** *202*, 750-757.

24. Kano, M.; Kokufuta, E. On the Temperature-Responsive Polymers and Gels Based on *N*-Propylacrylamides and *N*-Propylmethacrylamides. *Langmuir* **2009,** *25*, 8649-8655.

25. Tiktopulo, E. I.; Uversky, V. N.; Lushchik, V. B.; Klenin, S. I.; Bychkova, V. E.; Ptitsyn, O. B. Domain Coil-Globule Transition in Homopolymers. *Macromolecules* **1995,** *28*, 7519-7524.

26. Tang, Y. C.; Ding, Y. W.; Zhang, G. Z. Role of Methyl in the Phase Transition of Poly(*N*-isopropylmethacrylamide). *J. Phys. Chem. B* **2008,** *112*, 8447-8451.

27. Maeda, Y.; Nakamura, T.; Ikeda, I. Changes in the Hydration States of Poly(*N*-*n*-propylmethacrylamide) and Poly(*N*-isopropylmethacrylamide) during Their Phase Transitions in Water Observed by FTIR Spectroscopy. *Macromolecules* **2001,** *34*, 8246-8251.

28. Dybal, J.; Trchova, M.; Schmidt, P. The Role of Water in Structural Changes of Poly(*N*-isopropylacrylamide) and Poly(*N*-isopropylmethacrylamide) Studied by FTIR, Raman Spectroscopy and Quantum Chemical Calculations. *Vib .Spectrosc.* **2009,** *51*, 44-51.

29. Spěváček, J.; Dybal, J. Temperature-Induced Phase Separation and Hydration in Aqueous Polymer Solutions Studied by NMR and IR Spectroscopy: Comparison of Poly(*N*-vinylcaprolactam) and Acrylamide-Based Polymers. *Macromol. Symp.* **2014,** *336*, 39-46.

30. Kubota, K.; Hamano, K.; Kuwahara, N.; Fujishige, S.; Ando, I. Characterization of Poly(*N*-isopropylmethacrylamide) in Water. *Polym. J.* **1990,** *22*, 1051-1057.

31. Pang, J.; Yang, H.; Ma, J.; Cheng, R. S. Understanding Different LCST Levels of Poly(*N*-alkylacrylamide)s by Molecular Dynamics Simulations and Quantum Mechanics Calculations. *J. Theor. Comput. Chem.* **2011,** *10*, 359-370.

32. Vishnevetskaya, N. S.; Hildebrand, V.; Niebuur, B.-J.; Grillo, I.; Filippov, S. K.; Laschewsky, A.; Müller-Buschbaum, P.; Papadakis, C. M. "Schizophrenic" Micelles from Doubly Thermoresponsive Polysulfobetaine-*b*-Poly(*N*-isopropylmethacrylamide) Diblock Copolymers. *Macromolecules* **2017,** *50*, 3985-3999.

33. Heinz Maier-Leibnitz Zentrum; et al. KWS-1: Small Angle Scattering Diffractometer. *Journal of Large-Scale Research Facilities.* **2015,** *1*, A28.

34. Feoktystov, A. V.; Frielinghaus, H.; Di, Z. Y.; Jaksch, S.; Pipich, V.; Appavou, M. S.; Babcock, E.; Hanslik, R.; Engels, R.; Kemmerling, G.; Kleines, H.; Ioffe, A.; Richter, D.; Bruckel,

T. KWS-1 High-resolution Small-Angle Neutron Scattering Instrument at JCNS: Current State. *J. Appl. Crystallogr.* **2015,** *48*, 61-70.

35. Heinz Maier-Leibnitz Zentrum; et al. KWS-3: Very Small Angle Scattering Diffractometer with Focusing Mirror. *Journal of Large-Scale Research Facilities.* **2015,** *1*, A31.

36. Porod, G. Die Röntgenkleinwinkelstreuung von dichtgepackten kolloiden Systemen. *Kolloid Z.* **1951,** *124*, 83-114.

37. Teixeira, J. Small-Angle Scattering by Fractal Systems. *J. Appl. Crystallogr.* **1988,** *21*, 781-785.

38. Evmenenko, G.; Theunissen, E.; Mortensen, K.; Reynaers, H. SANS Study of Surfactant Ordering in Kappa-carrageenan/Cetylpyridinium Chloride Complexes. *Polymer* **2001,** *42*, 2907-2913.

39. Hammouda, B.; Ho, D. L.; Kline, S. Insight into Clustering in Poly(ethylene oxide) Solutions. *Macromolecules* **2004,** *37*, 6932-6937.

40. Shibayama, M.; Tanaka, T.; Han, C. C. Small-Angle Neutron-Scattering Study on Poly(*N*-isopropyl acrylamide) Gels near Their Volume-Phase Transition-Temperature. *J. Chem. Phys.* **1992,** *97*, 6829-6841.

41. Koberstein, J. T.; Morra, B.; Stein, R. S. Determination of Diffuse-Boundary Thicknesses of Polymers by Small-Angle X-Ray-Scattering. *J. Appl. Crystallogr.* **1980,** *13*, 34-45.

42. Schmidt, P. W. Interpretation of Small-Angle Scattering Curves Proportional to a Negative Power of the Scattering Vector. *J. Appl. Crystallogr.* **1982,** *15*, 567-569.

43. Beaucage, G.; Schaefer, D. W. Structural Studies of Complex-Systems Using Small-Angle Scattering - a Unified Guinier Power-Law Approach. *J. Non-Cryst. Solids* **1994,** *172*, 797-805.

44. Beaucage, G. Approximations Leading to a Unified Exponential Power-law Approach to Small-Angle Scattering. *J. Appl. Crystallogr.* **1995,** *28,* 717-728.

45. Grillo, I., *Small-Angle Neutron Scattering and Applications in Soft Condensed Matter.* Springer: Dordrecht, Netherlands, 2008.

46. Kline, S. R. Reduction and Analysis of SANS and USANS Data using IGOR Pro. *J. Appl. Crystallogr.* **2006,** *39,* 895-900.

47. Sánchez, M. S.; Hanyková, L.; Ilavský, M.; Pradas, M. M. Thermal Transitions of Poly(*N*-isopropylmethacrylamide) in Aqueous Solutions. *Polymer* **2004,** *45,* 4087-4094.

48. Meier-Koll, A.; Pipich, V.; Busch, P.; Papadakis, C. M.; Müller-Buschbaum, P. Phase Separation in Semidilute Aqueous Poly(*N*-isopropylacrylamide) Solutions. *Langmuir* **2012,** *28,* 8791-8798.

49. Maeda, Y.; Higuchi, T.; Ikeda, I. Change in Hydration State during the Coil-Globule Transition of Aqueous Solutions of Poly(*N*-isopropylacrylamide) as Evidenced by FTIR Spectroscopy. *Langmuir* **2000,** *16,* 7503-7509.

50. Ramon, O.; Kesselman, E.; Berkovici, R.; Cohen, Y.; Paz, Y. Attenuated Total Reflectance/Fourier Transform Infrared Studies on the Phase-Separation Process of Aqueous Solutions of Poly(*N*-isopropylacrylamide). *J. Polym. Sci. Pol. Phys.* **2001,** *39,* 1665-1677.

51. Ahmed, Z.; Gooding, E. A.; Pimenov, K. V.; Wang, L. L.; Asher, S. A. UV Resonance Raman Determination of Molecular Mechanism of Poly(*N*-isopropylacrylamide) Volume Phase Transition. *J. Phys. Chem. B* **2009,** *113,* 4248-4256.

52. Sun, B. J.; Lin, Y. A.; Wu, P. Y. Structure Analysis of Poly(*N*-isopropylacrylamide) using Near-Infrared Spectroscopy and Generalized Two-Dimensional Correlation Infrared Spectroscopy. *Appl. Spectrosc.* **2007,** *61,* 765-771.

53. Chaikin, P. M.; Lubensky, T. C., *Field Theories, Critical Phenomena, and the Renormalization Group. In Principles of Condensed Matter Physics*. Cambridge University Press: Cambridge, 1995; Chapter 5.

54. Onuki, A., *Critical Phenomena and Scaling. In Phase Transition Dynamics*. Cambridge University Press: Cambridge, 2002; Chapter 2.

55. Maiorano, A.; Martín-Mayor, V.; Ruiz-Lorenzo, J. J.; Tarancón, A. Weak First-order Transition in the Three-dimensional Site-diluted Ising Antiferromagnet in a Magnetic Field. *Phys. Rev. B* **2007,** *76*, 064435.

56. Graziano, G. On the Temperature-induced Coil to Globule Transition of Poly-*N*-isopropylacrylamide in Dilute Aqueous Solutions. *Int. J. Biol. Macromol.* **2000,** *27*, 89-97.

57. Zhang, Q. L.; Weber, C.; Schubert, U. S.; Hoogenboom, R. Thermoresponsive Polymers with Lower Critical Solution Temperature: from Fundamental Aspects and Measuring Techniques to Recommended Turbidimetry Conditions. *Mater. Horiz.* **2017,** *4*, 109-116.

58. Deshmukh, S. A.; Sankaranarayanan, S. K. R. S.; Suthar, K.; Mancini, D. C. Role of Solvation Dynamics and Local Ordering of Water in Inducing Conformational Transitions in Poly(*N*-isopropylacrylamide) Oligomers through the LCST. *J. Phys. Chem. B* **2012,** *116*, 2651-2663.